Photon-scattering-rate measurement of atoms in a magneto-optical trap

Kais Jooya,[1] Nam Musterer,[1] Kirk W. Madison,[1] and James L. Booth[2,*]

[1]*Department of Physics & Astronomy, University of British Columbia, 6224 Agricultural Road, Vancouver, British Columbia, Canada V6T 1Z1*

[2]*Physics Department, British Columbia Institute of Technology, 3700 Willingdon Avenue, Burnaby, British Columbia, Canada V5G 3H2*

(Received 30 August 2013; published 2 December 2013)

We present a technique for empirically determining the photon scattering rate of atoms in a magneto-optical trap (MOT). An accurate measurement of the scattering rate provides a way to accurately determine the number of atoms in the MOT, the excited-state fraction, and the *in situ* light intensity experienced by the atoms in the trap. We validate this technique for determining the scattering rate by comparing the atom number determined by the fluorescence emitted by atoms in a MOT with an independent and unrelated measure of the number determined by an absorption measurement of an optical pumping beam. We also observe minor deviations from the two-level model for the single-photon scattering rate and extend our analysis to a four-level model. The main advantage of the method described here is that it provides a simple way of determining the photon scattering rate of the MOT empirically and, thus, of evaluating the atom number from fluorescence measurements more accurately.

DOI: 10.1103/PhysRevA.88.063401 PACS number(s): 32.50.+d, 32.80.Xx, 37.10.Gh

I. INTRODUCTION

The production and study of ultracold atoms has led to significant breakthroughs in fundamental physics and the realization of a new class of quantum-degenerate matter including Bose [1–3], Fermi, and Bose-Fermi [4–10] gases, and to the formation of ultracold homonuclear and polar molecules [11–20]. Molecular Bose-Einstein condensates [21–23] have been realized, and high-precision studies of collisons between trapped atoms and other particles [24–28] have been facilitated. In addition, laser-cooled atoms have enabled the establishment of new primary standards and technological advances including the realization of ultraprecise atomic clocks [29,30] and ultrasensitive atomic interferometers used now for inertial guidance systems and gravimeters [31]. Miniaturization of this technology is currently under way [32–38], making this an exciting and productive area of research.

One of their main characteristics, making ultracold atoms such a versatile and attractive physical system for both fundamental and applied science, is the great degree of control and ease of measurement that they offer. Key to many applications is the ability to quantify the number of atoms in a dilute, cold ensemble from the measurement of the photons scattered by it. In the dilute limit, where the mean free path length of the photons is large compared to the ensemble size, the power scattered by the ensemble of cold atoms is

$$P_{\mathrm{scat}} = \gamma h\nu N_{\mathrm{e}} = \gamma_{\mathrm{sc}} h\nu N \tag{1}$$

where γ is the spontaneous decay rate of the atomic transition being excited, ν is the atomic transition frequency, N_{e} is the population of the atoms in the excited electronic state, and N is the total number of atoms in the magneto-optical trap (MOT). The photon scattering rate per atom, γ_{sc}, can be derived using the density matrix approach (for example, [39,40]) or the less general rate equation approach (for example, [41]). Both lead to the same prediction,

$$\gamma_{\mathrm{sc}} = \frac{\gamma}{2}\frac{s}{1+s+(2\Delta/\gamma)^2}. \tag{2}$$

In Eq. (2), $s = I/I_{\mathrm{sat}}$, where I is the intensity of the laser light experienced by the trapped atoms, I_{sat} is the saturation intensity of the atomic transition being observed, and Δ is the detuning of the laser frequency from the atomic resonance. While there exist other methods to determine the atom number (e.g., the absorption of an optical pumping beam [42]), Eqs. (1) and (2) are universally applied to estimate the atom number in a MOT based on a measurement of the average power of the fluorescent light signal emitted by it. Indeed, for sufficiently small atom numbers, the MOT fluorescence will exhibit quantized light levels allowing single-atom counting of the atoms in the MOT. Quite remarkably, recent work has shown that high-accuracy fluorescence measurements of atoms in a MOT allow for single-atom resolution of the atom number for ensembles as large as 1200, very near the quantum limit set by photon shot noise and atom number fluctuations due to trap loss [43]. With larger atom numbers where the quantization of the fluorescent power is obscured by noise, an accurate determination of the photon scattering rate is required to quantify the atom number. Therefore, in this work we investigate the above model and demonstrate a simple method to experimentally determine the *in situ* saturation parameter $s = I/I_{\mathrm{sat}} = P/P_{\mathrm{sat}}$, and, thus, the photon scattering rate of atoms in a magneto-optical trap.

The conceptual approach of this work is as follows: We begin by assuming that the standard two-level model for photon scattering rate is correct—a ubiquitous assumption in the literature but never empirically tested to our knowledge. We then use the fluorescence emitted from a fixed number of atoms under different illumination conditions to empirically determine the saturation parameter s. Based on the two-level model, the saturation parameter uniquely determines the scattering rate, and the atom number is simply the ratio of the total scattering rate to the per atom scattering rate. We then validate this empirical method of finding s by comparing the atom number in the MOT based on the number

*Corresponding author: James_Booth@bcit.ca

determined from an independent measurement technique using optical pumping. We find excellent agreement under certain conditions, but we also find evidence of the breakdown of the two-level model assumption. We extend our analysis to a four-level model and show that it more accurately reproduces the behavior of the MOT fluorescence as a function of the laser illumination frequency and power, and, thus, provides a more reliable estimate of the per atom scattering rate. We also show how the repump laser saturation parameter can be determined using the four-level model.

II. THEORY

The fluorescent light emitted by cold atoms contained in a MOT is one of the main diagnostic tools used to interrogate the atoms, their environment, and their interactions. This light is collected via an optical system of lenses and focused onto a photodetector which converts the photons into an electrical signal. The relationship between the fluorescent signal and the number of atoms in the MOT is

$$V = \alpha\gamma N_{\mathrm{e}}^{\mathrm{tot}}, \tag{3}$$

where V is the voltage signal produced by the photodetector, α is the photon collection efficiency of the optical system times the photon-to-voltage conversion factor for the detector, γ is the natural decay rate of the atomic transition, and $N_{\mathrm{e}}^{\mathrm{tot}}$ is the total atomic population in all of the excited states emitting photons. In general, the two-level model simplifies Eq. (3) to

$$V = \alpha\gamma_{\mathrm{sc}}N. \tag{4}$$

Here, there is only a single excited atom state considered responsible for the optical signal and γ_{sc} is given by Eq. (2). This model neglects any collective effects of photon scattering, a condition that has been shown to be true for small MOTs (i.e., dilute ensembles) but which breaks down at higher MOT densities and atom numbers [44–47]. Also, we neglect the Zeeman shifts experienced by the atoms due to the quadrupole magnetic field of the MOT. The main challenges to using Eq. (4) to deduce the atom number in the MOT are in estimating both α and γ_{sc}. Typically, one estimates

$$\alpha = e\left(\frac{\Omega}{4\pi}\right)ghv, \tag{5}$$

where $(\frac{\Omega}{4\pi})$ is the fraction of the total solid angle collected by the optical system, representing the maximum fraction of the scattered photons that can be collected, e is the transmission efficiency of the optical system accounting for loss through the optical components, g is the photon-energy-to-voltage conversion factor for the detector and recording system for photons of frequency, v. The latter can be calibrated directly. However, the first two factors are typically estimated as a calibration would require the introduction of an *in situ* photon source. Finally, the photon scattering rate per atom, γ_{sc}, is challenging to estimate as it relies on a knowledge of the *in situ* laser intensity at the location of the MOT. Estimating this intensity is complicated by reflection losses at the windows of the vacuum system, by the inevitable presence of beam imperfections such as interference fringes due to multiple reflections and diffraction rings, and by the effects of beam shadowing produced by the atoms in the case of retroreflection MOT beam configurations. Other authors [48–50] have also included the effects of partial optical pumping of the atoms in the MOT in Eq. (2) to provide a better description. This modification involves adding a factor C_1^2 multiplying the saturation parameter $s = I/I_{\mathrm{sat}}$ in the numerator of Eq. (2) and C_2^2 times s in the denominator. Towsend *et al.* [49] reported that the best description was $C_1^2 = C_2^2 = 0.73 \pm 0.1$ and $(C_1/C_2)^2 = 1 \pm 0.25$, for a cesium MOT. They also state that a Monte Carlo calculation for a cesium optical molasses yielded $C_1^2 = 0.9 \pm 0.1$.

In this work, we begin with the hypothesis that Eq. (4) is a good approximation and we demonstrate a ratiometric approach to determine the saturation parameter directly for atoms in a MOT over a wide range of intensities ($s = 7$ to 56 corresponding to pump laser powers ranging from 3 to 25 mW) and pump laser detunings in the range $\gamma \leqslant \Delta \leqslant 3\gamma$. We find that this determination provides an accurate measure of the photon scattering rate because the atom number we infer from it is in excellent agreement with the atom number determined by the absorption of an optical pumping beam. The method works as follows: the MOT is first loaded using preselected, convenient, "standard" settings for the "pump" and "repump" (defined below) laser powers and detunings, and for the magnetic field gradient. The steady-state fluorescence of the MOT is then measured using an optical collection system producing a voltage signal

$$V_{\mathrm{ss}}^{\mathrm{std}} = \alpha\gamma_{\mathrm{sc}}^{\mathrm{std}}N. \tag{6}$$

The trap conditions are then quickly shifted to different "test" settings, in a time (<1 ms) short compared to the time for the atom number in the MOT to change as it evolves to a new equilibrium number, and the fluorescence is recorded again:

$$V_{\mathrm{ss}} = \alpha\gamma_{\mathrm{sc}}N. \tag{7}$$

Taking the ratio of these two signals eliminates both the atom number and the detection efficiency α, to give an expression that depends solely on the ratios of scattering rates,

$$\frac{V_{\mathrm{ss}}^{\mathrm{std}}}{V_{\mathrm{ss}}} = \frac{\gamma_{\mathrm{sc}}^{\mathrm{std}}}{\gamma_{\mathrm{sc}}}. \tag{8}$$

Combining Eq. (8) with Eq. (2) we have

$$\frac{V_{\mathrm{ss}}^{\mathrm{std}}}{V_{\mathrm{ss}}} = \frac{s_{\mathrm{std}}}{s}\left[\frac{1+(2\Delta/\gamma)^2}{\zeta_{\mathrm{std}}} + \frac{1}{\zeta_{\mathrm{std}}}s\right]. \tag{9}$$

The term $\zeta_{\mathrm{std}} = 1 + s_{\mathrm{std}} + \left(2\Delta^{\mathrm{std}}/\gamma\right)^2$ is a common scaling factor determined by the user-selected standard MOT pump beam settings Δ_{std} and s_{std}.

The saturation parameter $s = I/I_{\mathrm{sat}} = P/P_{\mathrm{sat}}$, under the assumption that the pump laser power measured outside the MOT, P, is proportional to the intensity at the MOT, I, over the range of parameters tested. Thus, the ratio s_{std}/s in Eq. (9) can be expressed as P_{std}/P. It is important to emphasize that the power for the standard MOT setting, P_{std}, and the power for the test MOT setting, P, are both measured at a convenient location outside the vacuum cell. Inserting these into Eq. (9) one has

$$\frac{V_{\mathrm{ss}}^{\mathrm{std}}}{V_{\mathrm{ss}}} = \frac{P_{\mathrm{std}}}{P}\frac{1}{\zeta_{\mathrm{std}}}\left[[1+(2\Delta/\gamma)^2] + \frac{P}{P_{\mathrm{sat}}}\right]. \tag{10}$$

Finally, we define a parameter G, which simplifies the power dependence,

$$G = \frac{P}{P_{\rm std}}\frac{V_{\rm ss}^{\rm std}}{V_{\rm ss}} = \frac{1}{\zeta_{\rm std}}\left[[1+(2\Delta/\gamma)^2] + \frac{P}{P_{\rm sat}}\right]. \quad (11)$$

G is constructed from the experimentally measured quantities P, $P_{\rm std}$, $V_{\rm ss}^{\rm std}$, and $V_{\rm ss}$. This quantity provides a way to empirically determine the saturation power $P_{\rm sat}$ and, thus, the saturation parameter at any given laser power: Namely, using Eq. (11), one observes that, for a fixed pump laser detuning Δ, the two-level atom description of the per atom scattering rate predicts a linear relationship between G and the test laser power setting P. The corresponding slope m is

$$m = \frac{1}{\zeta_{\rm std}}\frac{1}{P_{\rm sat}} \quad (12)$$

and the intercept b,

$$b = \frac{1}{\zeta_{\rm std}}[1+(2\Delta/\gamma)^2]. \quad (13)$$

The empirical value for the parameter $P_{\rm sat}$ is then computed by combining Eqs. (12) and (13) as

$$P_{\rm sat} = \frac{b}{m[1+(2\Delta/\gamma)^2]}. \quad (14)$$

It is important to point out that $P_{\rm sat}$ is neither the saturation power at the MOT nor a direct measurement of the saturation intensity at the location of the MOT. Rather, $P_{\rm sat}$ corresponds to the laser power (measured outside the vacuum cell) that produces an illumination intensity at the atoms equal to $I_{\rm sat}$. Knowing $P_{\rm sat}$ allows one to infer the saturation parameter $s = I/I_{\rm sat} = P/P_{\rm sat}$ for the MOT at any other power, based on a two-level atom model. It is expected that $P_{\rm sat}$ (and, hence, s) will vary with the shape of the MOT (due to shadowing), with the trapping beam intensity imbalances, and with variations in beam spatial distributions, reflecting the local conditions in the trap.

As a further test of this analysis, one can relate the measured fluorescence signal V and the computed single-photon scattering rate per atom, $\gamma_{\rm sc}$, to the steady-state atom number in the MOT, Eq. (6). In some recent work [42] it was shown that the number of atoms in a MOT can be extracted by optically pumping the atoms into one hyperfine ground state (e.g., the $F = 3$ state for ^{85}Rb) and then applying a probe beam to the sample which is resonant with an electronic transition that can decay into either ground state. The result is that the atoms will be optically pumped into the dark state after scattering an average number of photons, ϕ, set by the branching ratio of the transitions to the two ground states. The optical pumping produces a time-dependent reduction of the probe beam intensity that lasts a few tens of microseconds. This signal can be recorded on a photodiode and compared to the signal observed with no atoms in the probe laser path. The difference between the two measurements provides a measure of the number of photons scattered, $N_{\rm sc}$, and, hence, $N = N_{\rm sc}/\phi$. The number of scattered photons is computed from the integrated area under the difference between the two curves, $\mathcal{A}$. Namely,

$$N = \frac{\mathcal{A}}{\phi h\nu}\frac{P_0}{V_0}. \quad (15)$$

In Eq. (15), ν is the frequency of the scattered photon, P_0 is the probe laser beam power, and V_0 is the signal measured on the photodetector at this power. This technique provides an independent measure of the atom number to compare against the number measured by the MOT fluorescence detection system. If Eqs. (6) and (14) are correct, plots of $V/\gamma_{\rm sc}$ versus MOT atom number N should converge along a common straight line for each of the chosen MOT pump laser powers. The slope of this plot will be an experimental determination of the photon collection efficiency times the photon-to-voltage conversion factor α.

III. EXPERIMENTAL SETUP

Our magneto-optical trap, described in [51], collects and cools rubidium atoms from a room-temperature Rb vapor (see Fig. 1). The light for the MOT is provided by a laser system composed of grating-stabilized and injection-seeded diode lasers [51,52]. In this work, the "standard" MOT settings corresponded to a total pump laser power of 18.0 mW ($P_{\rm std}$), red detuned by 12.0 MHz ($\Delta^{\rm std} \cong -2\gamma$) from the ($5\,^2S_{1/2} \rightarrow 5\,^2P_{3/2}$, $F = 3 \rightarrow F' = 4$) transition. The repump laser had a power of 0.56 mW, resonant with the ($5\,^2S_{1/2} \rightarrow 5\,^2P_{3/2}$, $F = 2 \rightarrow F' = 3$) transition. These two beams are combined and expanded to a $1/e^2$ horizontal (vertical) diameter of 7.4 (8.4) mm, prepared with the correct polarization, and introduced into the ($1 \times 1 \times 6$ cm^3) glass MOT vacuum cell along three mutually orthogonal axes in a retroreflection configuration. The MOT is operated with an axial magnetic field gradient of 27.9 (0.3) G cm^{-1}. The various laser detunings and intensities were set using computer-controlled acousto-optical modulators (AOMs), allowing for rapid ($\approx$3 μs) switching between different settings.

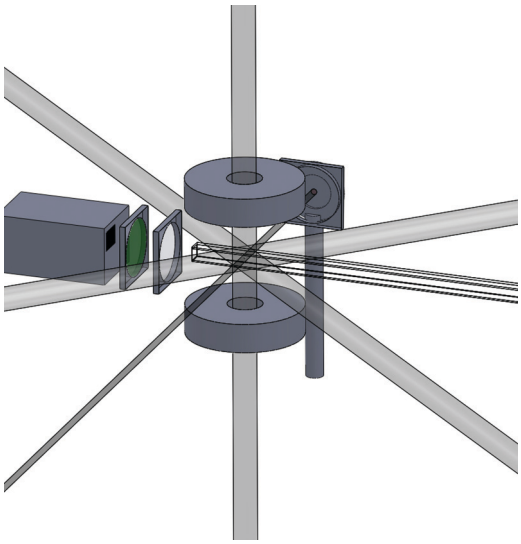

FIG. 1. (Color online) A schematic of the fluorescence detector, vapor cell, quadrupole magnets, MOT laser beams, and probe beam used in these experiments. The MOT was configured as a retroreflection MOT and in addition to the cooling and repump beams (the six laser beams shown intersecting in the center of the magnetic field coils), the probe laser is shown (drawn as the narrow laser entering the side face of the vacuum cell). See the text for details.

The measurement of the saturation parameter was carried out by holding the background rubidium density constant and filling a MOT using the standard pump and repump parameters (loading time on the order of 10 s). The standard fluorescence signal was recorded, V_{ss}^{std}, and the pump laser detuning and power were quickly switched to some preselected test values. The new fluorescence readings V_{ss} were taken just after the switch to ensure that the atom number in the MOT was the same for both measurements. From these data the parameter $G = (P/P_{std})(V_{ss}^{std}/V_{ss})$ was computed and plotted as a function of the test power P. It is important to point out that G was constructed based on Eq. (4), which assumes that $V \propto N$. For very large MOTs multiple scattering of photons may change the functional relationship between V and N for different pump and repump settings. While we did not observe any evidence of this for the MOTs studied in this work, it could be an important limitation of the technique presented in this paper. This work was limited by the power available for the laser beams and by the physical dimensions of the vacuum cell, excluding the investigation of very large MOTs. Here the number of atoms in the MOT was less than 15×10^6 atoms with peak densities ranging from 1.0×10^8 cm^{-3} to less than 1.0×10^{11} cm^{-3}.

The measurement of the MOT atom number by optical pumping was performed with a low-intensity probe beam. The probe beam was tuned on resonance with the ($5\,^2S_{1/2} \rightarrow 5\,^2P_{3/2}$, $F = 3 \rightarrow F' = 3$) transition. The beam was expanded to a diameter of approximately 2 cm and then passed through an iris to restrict its size to 4 mm as it entered the cell and intersected the cold atom cloud. The average intensity of this probe beam ranged from 1.2 to 2.0 mW cm^{-2}, in accordance with the parameters reported in [42]. After passing through the cell, the probe beam was collected by a lens and focused onto a high-speed photodiode (Thorlabs model PDA 155) to record the signal.

The goal of these investigations was to establish the relationship between the number of atoms in the MOT, N (determined via the probe beam absorption measurements), and the fluorescence signal detected, V. To achieve this, the rubidium density in the background vapour was increased by energizing a commercial rubidium dispenser for 2–3 min. This rapidly increased the rubidium density, the number of atoms captured in the MOT, and the fluorescence signal. To determine N, the MOT pump light was extinguished, followed by the repump light 0.3 ms later. This sequence ensured that the atoms were pumped into the $5\,^2S_{1/2}$ $F = 3$ ground state. Next the probe beam was sent through the cold atom cloud for 100 μs and the MOT light turned back on to recollect the atoms in the trap. With the same sample of atoms, this process was repeated and the results were averaged between 64 and 128 times to improve the signal-to-noise ratio. The MOT was then emptied and this process was repeated with no atoms in the trapping volume to provide the background probe light signal V_{bk}^{probe}, to compare with the scattered light signal V_{scat}^{probe}.

Signals from the MOT fluorescence photodiode and from the probe beam absorption photodiode were recorded on a Tektronix TDS 3014 digital oscilloscope and transferred to a computer. This device has excellent temporal resolution but is limited in its voltage resolution by its 8-bit analog-to-digital signal conversion. This is primarily a consideration when measuring the absorption out of the probe beam for low (a few million) atom numbers in the MOT. Repeated averaging of the signals, using the internal averaging function of the oscilloscope, helped to improve the signal-to-noise ratio. Each absorption measurement cycle took 20 ms, limited by the digitization rate of the oscilloscope. Therefore, it was important to perform these measurements on the equilibrium MOT to maintain a constant number of atoms. If the signal-to-noise ratio and the speed of the data acquisition were improved, this technique could be applied to obtain a direct measurement of $N(t)$ while the MOT was filling.

Care was taken here to ensure that the MOT had a spherical shape and did not shift its position by more than one diameter as the pump laser settings were varied. The MOT's spatial location was aligned with the zero of the magnetic quadrupole field by increasing the field and observing that the MOT did not shift its location significantly.

IV. RESULTS

The data will be presented in two sections. The first section describes the results of testing the two-level-atom model to predict the photon scattering rate using the parameter G introduced above. The dependence of G on the incident power provides a way to extract the empirical saturation power P_{sat}, which can then be used to evaluate the saturation parameter s and, subsequently, the photon scattering rate per atom, γ_{sc}.

The second section combines these results with an independent measurement of the atom number in a MOT [42]. The observed fluorescence signal V is correlated to the atom number N, to extract the photon collection efficiency times the photon-to-voltage conversion factor α.

A. Obtaining P_{sat} from MOT fluorescence measurements

The data acquisition proceeds as per the usual MOT capture process with the pump laser detuning and total power held fixed at preselected, convenient, standard settings. (Note: In the work reported here, the repump detuning and power as well as the quadrupole magnetic field gradient were held constant for these experiments.) Once the MOT had achieved steady-state conditions, the pump laser detuning and amplitude were quickly switched to a test setting, and the fluorescence values V_{std} and V_{test} were recorded. The MOT was then emptied by turning off the quadrupole magnetic field and the trapping lasers. Finally, the scattered light signals with no atoms present, V_{zero}^{std}, and V_{zero}^{test}, were measured with the trapping lasers on and the magnetic field off. The MOT fluorescence signals were then computed as

$$V_{ss}^{std} = V_{std} - V_{zero}^{std}. \tag{16}$$

V_{ss} for each test setting was computed in the same fashion. Figure 2 shows a typical recording of the steady-state fluorescence signals. In this figure, the voltage level for negative times ($t < 0.0$ s) corresponds to the fluorescence from the standard, steady-state MOT (V_{std}). The signal from $0.0 \leqslant t \leqslant 0.10$ s corresponds to the fluorescence of the same MOT under the test pump laser settings (V_{test}). During the time interval $0.1 \leqslant t \leqslant 0.2$ s the lasers and magnetic field were turned off

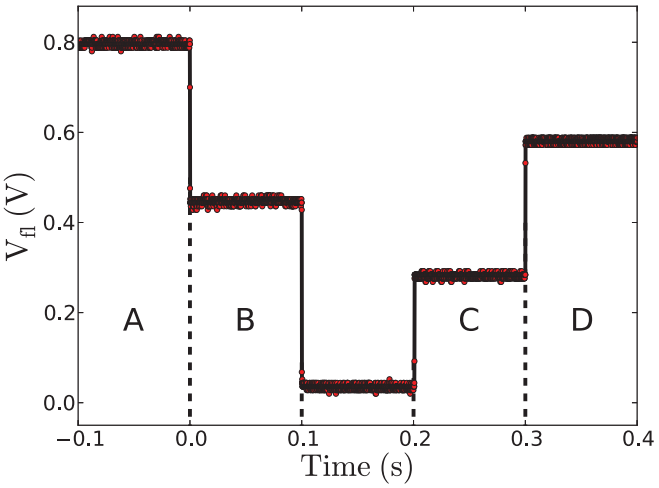

FIG. 2. (Color online) A plot of the scattered light from the MOT versus time. Section A is the fluorescence of the full MOT at the standard settings, and B shows the change in fluorescence when the pump laser detuning and power are rapidly switched to the test settings. Between B and C, the trapping lasers and the magnetic field were turned off to empty the atoms out of the trapping region. The trapping lasers were then turned back on to obtain a measurement of the scattered light signal at the test (C) and at the standard (D) settings, respectively.

to empty the MOT. Finally, in the range $0.2 \leqslant t \leqslant 0.3$ s the scattered light due to the test laser settings is recorded ($V_{\text{zero}}^{\text{test}}$), followed by a measurement of the scattered light due to the standard laser settings ($V_{\text{zero}}^{\text{std}}$).

At $t = 0.0$ s, when the pump laser settings are switched from the standard settings to the test settings, the equilibrium atom number may begin to change in response to the new trapping conditions. To obtain the best estimate of V_{test}, the voltage readings during the 0.1 s fluorescence measurement interval were linearly extrapolated back to the transition time $t = 0.0$ s. This extrapolation assumes that the equilibration time is long compared to the 0.1 s measurement time, as was observed for our data. For a rapidly changing fluorescence signal, an exponential decay model may be more appropriate.

Fluorescence measurements of this type were performed over a range of laser powers from 3 to 25 mW and at six different pump laser detunings: $\Delta/2\pi = -6.0, -8.0, -10.0, -12.0, -13.5,$ and -15.0 MHz. The parameter G as a function of laser power for each pump laser detuning is shown in Fig. 3. The linear trend predicted by Eq. (11) is evident.

The slopes and intercepts were extracted from these plots. The slopes m are plotted as functions of the pump laser detuning $|\Delta/2\pi|$ in Fig. 4. The slope is expected to be independent of laser detuning, but we observe a systematic increase (of about 12%) in the slope as the laser detuning increases from approximately 1γ to 2.5γ. This variation may be due to residual steering of the lasers emerging from the double-pass arrangement through the AOM causing slight variation in the laser power at the atoms and to the two-level-atom model's neglect of the effects of other atomic levels contributing to the measured fluorescence signal. It should be reiterated that the laser powers reported here were measured

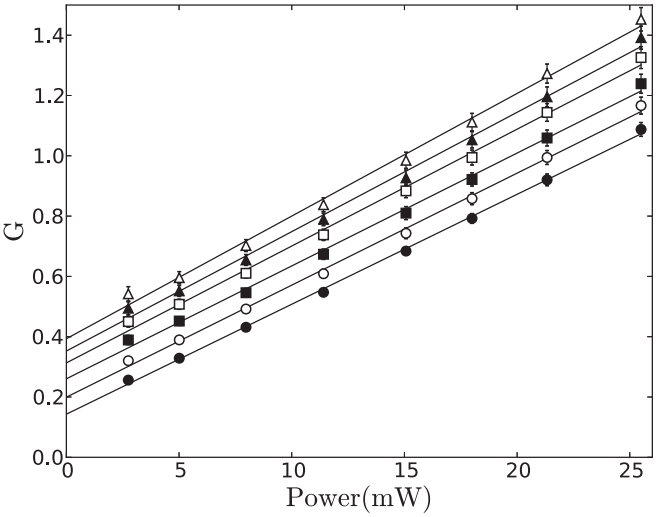

FIG. 3. A plot of the scattered light parameter G as a function of the pump laser test powers P. The different lines are linear fits to the data corresponding to detunings of $\Delta/2\pi = -6.0$ (•), -8.0 (○), -10.0 (■), -12.0 (□), -13.5 (▲), and -15.0 (△) MHz.

using a Coherent laser power meter (model PowerMax T0) at a location before the laser beams are split and sent along each trapping direction. The position is arbitrary and any convenient position can be used, provided that the laser power reaching the MOT is directly proportional to the power measured at the experimental location, $P_{\text{MOT}} \propto P$.

The values of the slopes and intercepts, and the parameters P_{sat} used to compute the saturation parameter s are reported in Table I. For ^{85}Rb, the spontaneous decay rate used in these calculations was $\gamma = 2\pi(5.7500)$ MHz [53].

To decide if these values fall within a reasonable range, we can estimate P_{sat} as follows: In the two-level model the parameter being estimated is $s = I/I_{\text{sat}}$. Following [49], the effects of optical pumping of the atoms in the MOT are incorporated by scaling s by the square of the effective Clebsch-Gordan coefficient C_2^2 in both the numerator and denominator of the two-level-atom scattering rate, giving $C_2^2 I/I_{\text{sat}}$. The relationship between the intensity of beam measured before the MOT vacuum cell and the intensity transmitted to the MOT apparatus is η. Further, once the MOT

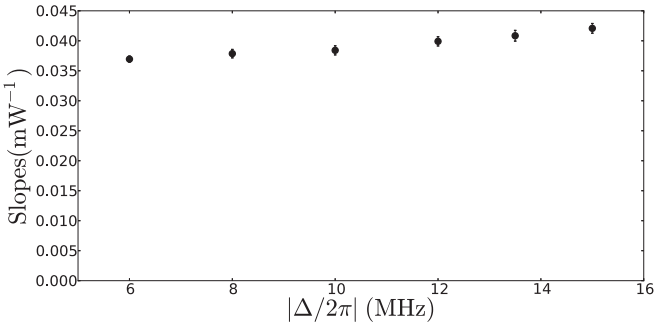

FIG. 4. A plot of the slopes of the scattered light parameter G as a function of the pump laser test powers P. The two-level-atom model predicts that these slopes should be constant as per Eq. (12). The increase in slope with increasing detuning is evidence for the breakdown of the two-level model as discussed below.

TABLE I. Measured slopes and intercepts from the plots of G as a function of pump laser power P for six different pump laser detunings. The effective saturation powers $P_{\rm sat}$ extracted from the slopes and intercepts are also reported.

Detuning (MHz)	Slope (mW^{-1})	Intercept	$P_{\rm sat}$ (mW)
−6	0.0365 (0.0005)	0.143 (0.008)	0.73 (0.04)
−8	0.0372 (0.0007)	0.199 (0.011)	0.61 (0.04)
−10	0.0374 (0.0009)	0.260 (0.013)	0.53 (0.03)
−12	0.0388 (0.0010)	0.313 (0.015)	0.44 (0.02)
−13.5	0.0396 (0.0011)	0.352 (0.016)	0.39 (0.02)
−15	0.0407 (0.0011)	0.393 (0.017)	0.34 (0.02)

beams pass through the cell they suffer losses at each window, β. In our retroreflection MOT configuration, this leads to a factor of β for the incoming beam and β^3 for the retroreflected beam. Thus the saturation parameter becomes

$$s = \frac{I}{I_{\rm sat}} = \frac{C_2^2[\eta\beta(1+\beta^2)]I}{I_{\rm sat}}. \tag{17}$$

Next the relationship between the peak intensity and the total power in a Gaussian beam can be applied, $I = 2P/\pi w^2$, where w is the beam radius. The pump laser beam $1/e^2$ diameters in the horizontal and vertical directions were $D_h = 7.4$ mm and $D_v = 8.4$ mm, respectively. The radii can be estimated as $w_i = D_i/(1.224)(2)$. The factor of 1.224 derives from the definition of the Gaussian radius of the beam (capturing 86.5% of the beam power) compared to the aperture capturing 95% of the beam power. For this work, $w_h = 0.30$ cm and $w_v = 0.34$ cm. Combining these gives

$$\frac{I}{I_{\rm sat}} = C_2^2[\eta\beta(1+\beta^2)]\frac{2P}{\pi w_h w_v}\frac{1}{I_{\rm sat}}. \tag{18}$$

Finally, one can estimate $P_{\rm sat}$,

$$P_{\rm sat} = \frac{\pi w_h w_v I_{\rm sat}}{2C_2^2[\eta\beta(1+\beta^2)]}. \tag{19}$$

Using $I_{\rm sat} = 3.896\ \mathrm{mW\,cm^{-2}}$ [53], one can compute $P_{\rm sat} = 0.66(0.20)$ mW. While this estimate has a large uncertainty owing to uncertainties in the beamwidths (5%), transmission losses through the glass cell, β (10%), and the uncertainty in the value for C_2^2 (25%), it is in agreement with the values reported in Table I.

From these results, we see that the inferred value for the single-atom scattering rate $\gamma_{\rm sc}$ has a precision that is better than 5%. At higher saturation parameters the precision is higher as s dominates the numerator and denominator in the expression Eq. (2), while at lower saturation parameters, the precision is limited by the precision of the measured $P_{\rm sat}$ value. This technique offers a precise, measured value for $\gamma_{\rm sc}$.

As a final test of the two-level model, Eq. (11) predicts that the intercepts for each detuning in Fig. 3 should scale linearly with $1 + (2\Delta/\gamma)^2$, with a slope $m_{\rm intcpt}$ of

$$m_{\rm intcpt} = \frac{1}{\zeta_{\rm std}} = \frac{1}{1 + \mathrm{I}^{\rm std}/\mathrm{I}_{\rm sat} + (2\Delta^{\rm std}/\gamma)^2}, \tag{20}$$

and should have a zero intercept. The results, shown in Fig. 5, show a small nonlinearity as well as a nonzero intercept. This is further evidence of the limitations of the simple model which does not take into account the multilevel structure of the atoms.

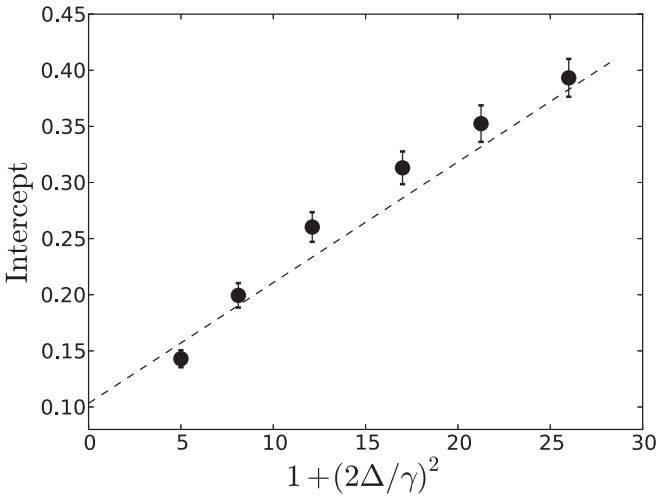

FIG. 5. A plot of the intercepts from Fig. 3 as a function of $1 + (2\Delta/\gamma)^2$. As expected from Eq. (12), these two quantities are linearly related but we also observe an additional, small, nonlinearity.

B. Correlation of MOT atom number and fluorescence signal

Armed with this experimental method for determining the saturation parameter and the two-level atom scattering rate for a MOT, one can test this prescription by correlating MOT fluorescence measurements with MOT atom number [Eq. (4)]. As described above, the number of atoms in the steady-state MOT can be measured independently using the technique described in [42]. To count the atom number in a steady-state MOT, the atoms were optically pumped into the $F = 3$ ground state by extinguishing the pump laser while leaving on the repump laser for 0.3 ms. The repump laser was then turned off and a probe beam, tuned on resonance with the $F = 3$-$3'$ transition, was flashed on the MOT. This beam had a diameter of 4 mm and an average intensity in the range of 1.2 to 2.0 $\mathrm{mW\,cm^{-2}}$. As described in [42], it is not necessary to turn off the magnetic field to perform this measurement, simplifying the experimental arrangement.

This probe light was collected onto a fast photodiode and the signal collected over 100 μs. The probe light is absorbed by the atoms in the $F = 3$ ground state and pumps them into the dark $F = 2$ state after scattering an average of $\phi = 2.25$ photons. We have checked with Mont Carlo simulations that ϕ is the same, independent of the initial $F' = 3$ magnetic sublevel population. This means that even in the presence of varying state populations due to changing MOT conditions, the analysis given in [42] remains valid. This scattering is observed as a "bite" out of the probe light signal. In this work, the number of atoms collected is relatively small and the data collection was limited by an 8-bit vertical resolution oscilloscope (Tektronix TDS 3014). The resulting difference in the two traces, approximated as an exponential decay curve, was typically only a few millivolts on a 400 mV background. The probe beam measurement was averaged between 64 and 128 times for each MOT sampled. Figure 6 illustrates the traces for a MOT containing approximately 14×10^6 atoms. The bit

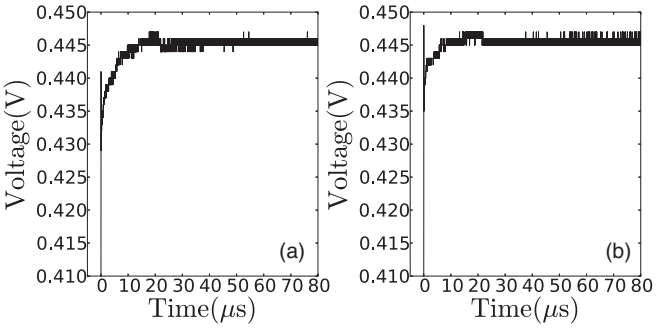

FIG. 6. The optical pumping beam intensity as a function of time. (a) shows the probe beam intensity when the MOT contains atoms, while (b) indicates the absorption when no atoms are present. The atoms being optically pumped into the $5\,^2S_{1/2}$ $F = 2$ state scatter photons out of the probe beam, producing the initial dip seen in (a).

resolution is clearly seen. The difference trace (Fig. 7) was fitted to an exponential form,

$$V_{\text{diff}} = V_a e^{-t/\tau} + V_b, \tag{21}$$

where V_a is the amplitude of the signal, τ is the observed decay time constant, and V_b is the equilibrium difference voltage level when all the atoms have been optically pumped into the $F = 3$ state. Ideally, V_b is zero, but varied here as the probe beam intensity drifted over time from pulse to pulse and between each pulse averaging sequence. Although these drifts were not large, even a 0.5% intensity variation can lead to a significant residual equilibrium value V_b (± 1 bit). To minimize this effect any residual value V_b was removed and the area under the curve was computed as $\mathcal{A} = V_a\tau$. The atom number was then calculated as per Eq. (15). Note that this drift gives rise to a significant limitation when applying this probe beam absorption measurement to a MOT with fewer than a few million atoms. In this work, a conservative uncertainty of $\pm 1.0 \times 10^6$ atoms was assigned to the probe beam measurements.

To correlate the MOT fluorescence with the atom number measurement, the rubidium dispenser was electrically heated for a short duration (2–3 min). This increased the density of the rubidium atoms in the trapping region, resulting in a greater number of atoms trapped in the MOT. As the ion pump attached to the system slowly removed rubidium from the test chamber,

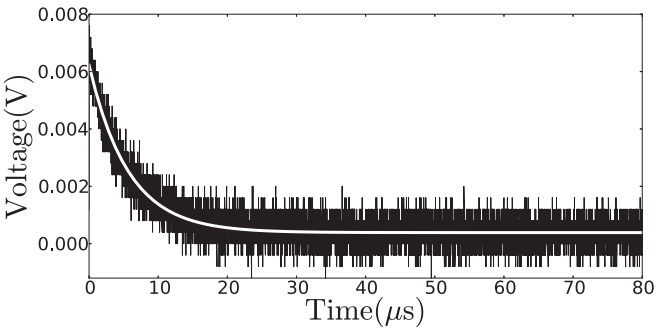

FIG. 7. The difference between the two probe beam absorption traces was fitted to a an exponential decay (solid line). The area under the difference plot is a measure of the number of photons scattered out of the probe beam.

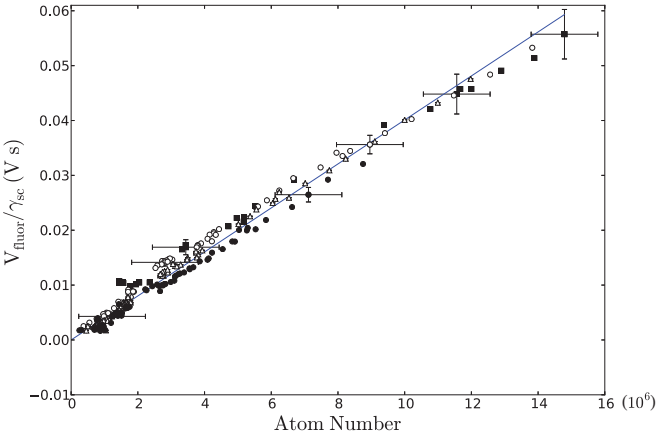

FIG. 8. (Color online) A plot of the MOT fluorescence signal normalized by the single-atom scattering rate V/γ_{sc} as a function of the atom number in the MOT determined from the optical pumping beam absorption. For these data the pump laser detuning was held fixed at $\Delta/2\pi = -12$ MHz while the MOT fluorescence was recorded using four different pump powers, 5.0 mW (■), 11.4 mW (△), 18.0 mW (○), and 25.5 mW (●). Sample error bars are shown on the plot for several data points. The solid line is a linear fit to all the data points, constrained to pass through the origin.

the background rubidium density and the steady-state MOT number decreased over time. Measurements of the steady-state MOT fluorescence using a pump laser beam detuned 12 MHz below resonance with the ^{85}Rb $5\,^2S_{1/2}$-$5\,^2P_{3/2}$, $F = 3 \rightarrow F' = 4$ transition at four different pump laser powers 5.0, 11.4, 18.0, and 25.5 mW, were recorded. These MOT fluorescence voltages were normalized by the two-level model for the scattering rate Eq. (2), using a value of $P_{\text{sat}} = 0.43(2)$ mW, extracted as previously described. The relationship between the normalized MOT fluorescence voltages and the measured atom numbers is shown in Fig. 8. The data points converge to a common line within experimental uncertainty, in agreement with the model,

$$\frac{V}{\gamma_{\text{sc}}} = \alpha N. \tag{22}$$

The slope of this plot provides a measure for the light collection efficiency and the photon-to-voltage conversion factor $\alpha = 4.01(2) \times 10^{-15}$ V s. For comparison we follow the standard estimation procedure [see Eq. (5)]: $(\frac{\Omega}{4\pi}) = 8.3(7) \times 10^{-3}$, and the photon-energy-to-voltage conversion factor was measured to be $g = 21.6(2)$ V/μW to give $\alpha_{\text{est}} = e[4.6(4) \times 10^{-14}]$ V s. The transmission factor of the MOT vacuum cell window and the lens focusing the MOT light onto the photodiode is estimated as $t_1 = 0.72(0.10)$. Finally, a neutral-density filter was used in the optical collection system which ensured that the fluorescent light did not saturate the detector over the entire range of atom number studied. The filter's transmission factor was measured to be $t_2 = 0.15(0.01)$, and, thus, $e = t_1 t_2 = 0.109(0.017)$. This gave the estimated value $\alpha_{\text{est}} = 5.0(0.9) \times 10^{-15}$ V s. Note that the measured factor has an uncertainty that is an order of magnitude better than the estimated value. The estimated value is higher than the measured result, probably due to an overestimate of the optical transmission and the solid angle collected.

V. EXTENSION OF MODEL TO A FOUR-LEVEL SYSTEM

We have demonstrated that this experimental technique for measuring the saturation parameter together with the simple two-level model provides a reliable value for the scattering rate in the MOT by finding good agreement between the atom numbers determined by fluorescence and optical pumping measurements. However, we do observe slight deviations of the dependence of G on detuning from the predictions of the two-level model. We believe these deviations arise from hyperfine pumping effects. Fortunately, although this breakdown of the two-level model produces a variation of the empirically determined value for $P_{\rm sat}$ for different detunings, we find that the scattering rate inferred from $P_{\rm sat}$ is still a reliable quantity under the conditions of this work. It is nevertheless instructive to investigate why these variations occur and when the simple two-level model predictions are no longer reliable.

Based on our model Eq. (11), plots of G as a function of pump laser power P for different detunings should yield linear relationships. The simple two-level model also predicts that the slopes should be independent of the pump laser detuning and that the intercepts should scale with $[1+(2\Delta/\gamma)^2]$. By contrast, our observations show that the slopes vary with pump laser detuning. This is not surprising since the pump light can nonresonantly excite a transition to the $F'=3$ state, leading some atoms to decay into the $F=2$ state. Once in this state, the fluorescence is determined by the repump light until the atom returns to the $F=3$ hyperfine state.

To include these processes, we model the atom as a simple four-level system. The pump laser transfers atoms from the $(F=3)$ ground state to the $(F'=4)$ excited state. The pump can also excite atoms nonresonantly to the $(F'=3)$ (or other levels) which leads to a transfer of atoms to the dark, $(F=2)$ ground-state level. The repump laser excites atoms from the $(F=2)$ to the $(F'=3)$ state, fluorescing as the atoms return to one or the other ground atomic levels. In the model presented below, n_1, n_2, n_3, and n_4 refer to the atoms in the $F=2$, $F=3$, $F'=3$, and $F'=4$ states, respectively:

$$\begin{aligned} n_1 &= -\Gamma_{13}n_1 + (\Gamma_{13}+\gamma/2)n_3, \\ n_2 &= -\Gamma_{23}n_2 - \Gamma_{24}n_2 + (\Gamma_{24}+\gamma)\,n_4 + (\Gamma_{23}+\gamma/2)\,n_3, \\ n_3 &= \Gamma_{13}n_1 + \Gamma_{23}n_2 - (\Gamma_{13}+\gamma)\,n_3, \\ n_4 &= \Gamma_{24}n_2 - (\Gamma_{24}+\gamma)\,n_4. \end{aligned} \tag{23}$$

In these equations the Γ_{ij} refer to the laser-induced coupling between levels i and j and γ is the natural decay rate of the excited atomic levels. For simplicity here, the branching ratio for decays $F'=3\rightarrow F=3$ is approximated as equal to the branching ratio from the $F'=3$ to the $F=2$ state. In steady state, under the assumption of a constant atom number $N=\Sigma_i n_i$, these equations can be solved for the populations in each atomic level, n_i.

Since the fluorescence signal detected is proportional to the population of atoms in the excited states, namely, n_3 and n_4, these solutions are pertinent,

$$n_3 = \frac{2\Gamma_{23}}{\gamma}\frac{N}{D} \tag{24}$$

and

$$n_4 = \frac{\Gamma_{24}/\gamma}{(1+\Gamma_{24}/\gamma)}\frac{N}{D} \tag{25}$$

with

$$D = 1+\frac{\Gamma_{23}}{\Gamma_{13}}\left(1+\frac{2\Gamma_{13}}{\gamma}\right)+\frac{2\Gamma_{23}}{\gamma}+\frac{\Gamma_{24}/\gamma}{(1+\Gamma_{24}/\gamma)}. \tag{26}$$

In the expressions above, Γ_{13} is the rate at which atoms are resonantly excited by the repump laser from the $F=2$ to the $F'=3$ level. Γ_{24} is the pump-laser-induced excitation rate of atoms from the $F=3\rightarrow F'=4$ cooling transition. Γ_{23} is the highly blue-detuned excitation rate of atoms from $F=3$ to the $F'=3$ state by the pump laser. The fluorescence detected by the photodetector is

$$V = \alpha\gamma(n_4+n_3). \tag{27}$$

Equation (27) is simply a restatement of Eq. (3), explicitly including the two excited states used in this four-level model. Typically, Γ_{23} is a small quantity compared to either Γ_{13} or Γ_{24}. In the limit $\Gamma_{23}\rightarrow 0$, then $n_3\rightarrow 0$ and the usual two-level-model solution is recovered.

The interpretation of the experimental parameter $G=(P/P_{\rm std})(V_{\rm ss}^{\rm std}/V_{\rm ss})$ is modified under the four-level model. Namely,

$$G = \frac{1}{\zeta_{\rm std}}\left[[1+(2\Delta/\gamma)^2]\left(1-2\epsilon\frac{A}{B}\right)+\frac{P}{P_{\rm sat}}\left(1+\epsilon(k-3)\frac{A}{B}\right)\right]. \tag{28}$$

Here $A=[1+(2\Delta/\gamma)^2]$, $B=\{1+[2(\Delta_{\rm hf}+\Delta)/\gamma]^2\}$, and $\Delta_{\rm hf}$ is the energy difference between the $F'=3$ and $F'=4$ hyperfine atomic levels of the $5\,^2P_{3/2}$ manifold, 120.640(68) MHz for ^{85}Rb [53]. ϵ is the ratio of the saturation intensity for the $F=3\rightarrow F'=4$ pump transition, $I_{\rm sat}^{3\text{-}4'}$, to the saturation intensities for the $F=3\rightarrow F'=3$ transition, $I_{\rm sat}^{3\text{-}3'}$. The parameter $k=(1+2I_r/I_{\rm sat}^r)/(I_r/I_{\rm sat}^r)$, introduces some dependence on the repump laser intensity I_r into the measured fluorescence signal. (The details of this calculation are provided in the Appendix.)

The consequences of the four-level model can be appreciated by comparing Eq. (28) to the two-level-atom model interpretation, Eq. (11). Under the four-level-atom model, using a fixed pump laser detuning Δ, G remains linearly proportional to the pump laser power P and has an intercept proportional to $[1+(2\Delta/\gamma)^2]$. However, these are modified by the parameters $\epsilon A/B$, which measure the relative effect of the pump laser exciting atoms to the $F'=4$ state (cooling transition) compared to excitation to the $F'=3$ level—a process that is ignored in the two-level model. Specifically the four-level-atom model G vs P slope is

$$m^{(4)} = \frac{1}{\zeta_{\rm std}}\frac{1}{P_{\rm sat}}\left(1+\epsilon(k-3)\frac{A}{B}\right) \tag{29}$$

and the corresponding intercept is

$$\begin{aligned} b^{(4)} &= \frac{1}{\zeta_{\rm std}}[1+(2\Delta/\gamma)^2]\left(1-2\epsilon\frac{A}{B}\right) \\ &= \frac{1}{\zeta_{\rm std}}A\left(1-2\epsilon\frac{A}{B}\right). \end{aligned} \tag{30}$$

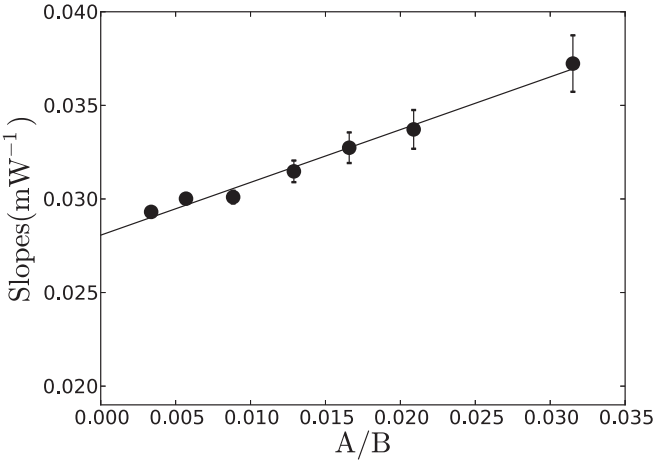

FIG. 9. A plot of the observed slopes $m^{(4)}$ as functions of $A/B = [1 + (2\Delta/\gamma)^2]/\{1 + [2(\Delta_{\rm hf} - \Delta)/\gamma]^2\}$. In agreement with the model Eq. (28), there should be a linear relationship between these two quantities.

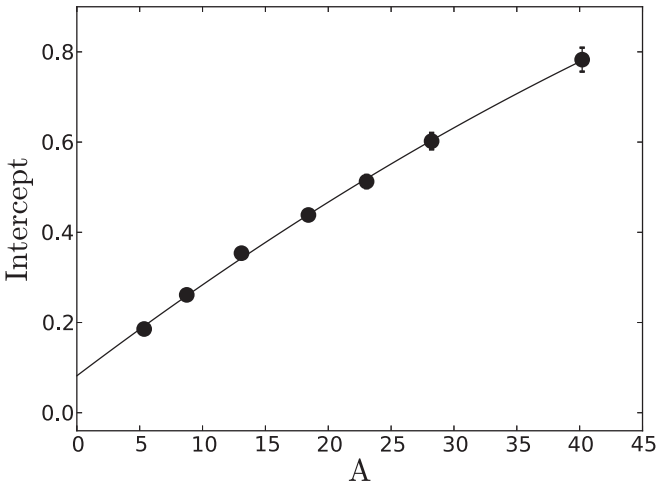

FIG. 10. A plot of the observed intercepts $b^{(4)}$ as functions of $A = [1 + (2\Delta/\gamma)^2]$. The solid curve is a quadratic fit to the data.

Equation (29) predicts that the slope of G versus the pump power P at a fixed pump laser frequency detuning is not the constant value predicted by the two-level-model approximation, but will vary with detuning through the $\epsilon(k-3)\frac{A}{B}$ term. This dependence can be positive, negative, or zero, depending on the ratio of the repump intensity to its saturation intensity. ($k > 3$ when $I_r/I^r_{\rm sat} < 1.0$, $k = 3$ when $I_r/I^r_{\rm sat} = 1.0$, and $k = 2$ when $I_r/I^r_{\rm sat} \to \infty$) Thus, a systematic study of the slope of G versus P for different repump powers presents a method for tuning the repump power into saturation. This revised model also predicts that the intercepts observed for these plots of G versus P at each detuning will be $A(1 - 2\epsilon\frac{A}{B})$, a more complicated function of the detuning.

Subsequent measurements were carried out and the slopes and intercepts of G versus P plots were determined. As before, the repump power and magnetic field gradient were held fixed. Figure 9 displays the slopes as a function of A/B. The linear relationship agrees with the prediction of Eq. (29). The corresponding intercepts as a function of A are shown in Fig. 10. The fit curve shown is quadratic in A, in accordance with Eq. (30).

The saturation power extracted using the ratio of the intercept to the slope of the G versus P plots for different pump laser detunings, as per Eq. (19), is now predicted to be a function of the pump laser detuning and the parameter :

$$P^{(4)}_{\rm sat}(\Delta,k) = \frac{b^{(4)}}{A\, m^{(4)}} = P_{\rm sat}\frac{1 - 2\epsilon\frac{A}{B}}{1 + \epsilon(k-3)\frac{A}{B}}, \qquad (31)$$

where $P_{\rm sat}$ is the value one would expect for a perfect two-level system. $P^{(4)}_{\rm sat}$, the empirically determined saturation power, is manifestly detuning dependent. When it is used with the two-level model [Eq. (2)], we see that the scattering rate prediction is different from the four-level-model scattering rate. That is, the two-level atom $\gamma_{\rm sc}$, computed with $P^{(4)}_{\rm sat}$, is

$$\gamma_{\rm sc} = \frac{\gamma}{2}\frac{s'}{s' + [1 + (2\Delta/\gamma)^2]} = \frac{\gamma}{2}\frac{s'}{s' + A}, \qquad (32)$$

where $s' = P/P^{(4)}_{\rm sat}$. This contrasts with the four-level-model expression for the scattering rate,

$$\gamma^{(4)}_{\rm sc} = \frac{\gamma}{2}\frac{s}{s\left[1 + \epsilon(k-3)\frac{A}{B}\right] + A\left(1 - 2\epsilon\frac{A}{B}\right)} = \frac{\gamma}{2}\frac{s'}{s' + A}\frac{1}{\left[1 + \epsilon(k-3)\frac{A}{B}\right]}. \qquad (33)$$

Comparing (32) to (33), one observes that the two-level-model prediction for the single-photon scattering rate is a factor of $[1 + \epsilon(k-3)\frac{A}{B}]$ times the four-level-model prediction. In the limit that the repump intensity is much larger than its saturation intensity, $I_r \gg I^r_{\rm sat}$, we find that $k \to 2$ and the two-level-model scattering rate prediction underestimates the actual scattering rate (more accurately quantified by the four-level model). However, when the repump intensity is smaller than the saturation intensity $I_r < I^r_{\rm sat}$, $k > 3$ and the two-level-model scattering rate prediction overestimates the scattering rate. It is interesting to note that when the repump intensity is exactly equal to the saturation intensity $I_r = I^r_{\rm sat}$, the slopes of G versus P are independent of detuning and the scattering rate predicted by the two-level model agrees with that of the four-level model.

In this work, we estimate that $k \approx 4$, so that the two-level scattering rate using $P^{(4)}_{\rm sat}$ calculated as per the prescription reported is a slight overestimate of the actual scattering rate assumed to be given by the four-level model. Specifically, for the range of detunings investigated here, $\Delta < 4\gamma$, the scattering rate determined by the two-level model overestimates the actual scattering rate by less than 3%. It is important to point out that as the detuning increases, the ratio A/B increases, and this systematic error in the two-level-model prediction increases, illustrating a serious limitation of the two-level model at large detunings.

Here, where small detunings were explored and the repump intensity was nearly equal to its saturation intensity, it is not surprising that we found excellent agreement between the atom number determination based on optical pumping with that based on fluorescence measurements and the two-level-model scattering rate prediction. We conclude that the two-level

model can be used with care but, in general, the four-level model presented here should produce a better prediction of the scattering rate over a wider range of parameters. We note that the four-level model presented here does not predict all of the observations. Specifically, the behavior of the intercept as $A \to 0$ in Fig. 10 is not in agreement with Eq. (28). The implications of this are the topic of future work.

VI. CONCLUSIONS

In this paper we have described a simple experimental method to measure the atom saturation parameter and empirically deduce the photon scattering rate of atoms in a MOT. This method can be applied in any standard MOT apparatus and can improve the precision with which the atom number is estimated.

There are two main advantages to the method presented: First, this measurement scheme to determine the saturation parameter obviates the need to estimate the intensity of the trapping lasers in the MOT and it automatically incorporates optical pumping corrections [49]. This parameter can be used to determine the photon scattering rate of atoms in the MOT using the two-level model with a precision of better than 5%. We show that the use of the two-level model will introduce a systematic error to the scattering rate prediction that can be minimized by choosing the repump laser intensity as $I_r \approx I_{\text{sat}}^r$, and this intensity regime for the repump laser illumination can be found empirically by measuring the dependence of the parameter G on power and detuning. The saturation parameter thus determined also provides a measure of the excited-state fraction of atoms in the MOT. Use of the four-level model discussed here will produce a more accurate determination of both the scattering rate and the excited-state fraction. Second, when combined with an independent measure of the trapped atom number [42], the calibration of the optical detection system can be measured with a precision of better than 1%. Finally, we find that by using the determined values for γ_{sc} and α, the MOT fluorescence measurements can be used to determine the atom number with a precision of 5%, for the dilute MOTs studied here.

If one were solely interested in the determination of total atom number, then the probe beam absorption method provides a similar precision [42] to that of the MOT fluorescence measurements presented here, for large atom numbers. However, the optical pumping measurement is not well suited for small samples at low density, and, in our work, the signal-to-noise ratio is inferior to that for a fluorescence measurement at sample sizes of less than a few million atoms.

It would be very interesting to apply this procedure to MOTs with large numbers of atoms ($N > 10^8$), where the effects of multiple scattering of the photons are significant. This might reveal a nonlinear relationship between the measured fluorescent signal and the atom number in the MOT. Owing to the limited laser power available and to the small size of our vacuum chamber, this regime could not be investigated during the present study.

ACKNOWLEDGMENTS

The authors acknowledge financial support from the Canadian Institute for Advanced Research (CIfAR), the Natural Sciences and Engineering Research Council of Canada (NSERC/CRSNG), the Canadian Foundation for Innovation (CFI), and the British Columbia Institute of Technology (BCIT) School of Computing and Academic Studies. This work was done under the auspices of the Center for Research on Ultra-Cold Systems (CRUCS).

APPENDIX: FOUR-LEVEL-ATOM MODEL

As stated in Sec. V, the four-level-atom model presented in Eq. (23) can be solved in the steady state for the equilibrium populations of the $F' = 4$ state, n_4, and the $F' = 3$ state, n_3 [Eqs. (24) and (25)]. Both of these are proportional to the total number of atoms in the MOT ($N = n_1 + n_2 + n_3 + n_4$) divided by a common denominator D [Eq. (26)], which includes the pump-laser-induced transition rates for the $F = 3 \to F' = 4$ transition, Γ_{24}, and for the $F = 3 \to F' = 3$ transition, Γ_{23}, and the resonant repump-laser-induced transition rate ($F = 2 \to F' = 3$), Γ_{13}. To implement the four-level model, one explicitly includes the dependence on the pump laser detuning from the $F = 3 \to F' = 4$ transition, Δ, in these rate constants [41],

$$\Gamma_{13} = \gamma \left(\frac{I_r}{2I_{\text{sat}}^r} \right), \tag{A1}$$

$$\Gamma_{24} = \gamma \left(\frac{I}{2I_{\text{sat}}} \right) \frac{1}{1 + (2\Delta/\gamma)^2} \tag{A2}$$

$$\Gamma_{23} = \gamma \left(\epsilon \frac{I}{2I_{\text{sat}}} \right) \frac{1}{1 + [2(\Delta_{\text{hf}} + \Delta)/\gamma]^2}, \tag{A3}$$

where Δ_{hf} was defined in Sec. V as the energy difference between the $F' = 3$ and $F' = 4$ hyperfine atomic levels of the $5^2P_{3/2}$ manifold. I is the intensity of the pump laser, and I_r is the repump laser intensity. Each atomic transition will have a different saturation intensity [53]. These are labeled as I_{sat}^r for the repump transition, while for the pump transition ($F = 3 \to F' = 4$) I_{sat} is used. As explained previously, ϵ is the ratio of the saturation intensities for the $F = 3 \to F' = 4$ to $F = 3 \to F' = 3$ transitions. Expressions (A1)–(A3) can be simplified using the substitutions $A = 1 + (2\Delta/\gamma)^2$, $B = 1 + [2(\Delta_{\text{hf}} + \Delta)/\gamma]^2$, and $s = I/I_{\text{sat}}$. Inserting these into the expression for the fluorescence signal, $V = \alpha\gamma(n_3 + n_4)$, one obtains

$$V = \frac{\alpha\gamma}{2} \frac{s}{A + s} \frac{W}{H}. \tag{A4}$$

Here,

$$W = \left(1 + \frac{2\epsilon \left(A + \frac{s}{2} \right)}{B} \right), \tag{A5}$$

$$H = \left(1 + \left[\frac{1 + \frac{2I_r}{I_{\text{sat}}^r}}{\frac{I_r}{I_{\text{sat}}^r}} \right] \left[\frac{\epsilon s}{B} \right] \left[\frac{A + \frac{s}{2}}{A + s} \right] \right). \tag{A6}$$

In Eq. (A6) one observes the emergence of the parameter k defined in Sec. V,

$$k = \frac{1 + \frac{2I_r}{I_{\text{sat}}^r}}{\frac{I_r}{I_{\text{sat}}^r}}, \tag{A7}$$

which introduces an explicit dependence on the repump laser into the fluorescence measurement.

From Eqs. (A4)–(A7), one can construct $G = (P/P_{\rm std})(V_{\rm ss}^{\rm std}/V_{\rm ss})$,

$$G = \frac{1}{\zeta_{\rm std}}(A+s)\frac{H}{W}. \tag{A8}$$

The normalization factor in Eq. (A8) $\zeta_{\rm std} = [1 + \frac{I}{I_{\rm sat}} + (\frac{2\Delta}{\gamma})^2]H/W$ where the user-selected standard values for the laser intensities and detunings are inserted.

Equations (A5)–(A8) can be combined, $s = I/I_{\rm sat}$ replaced by $s = P/P_{\rm sat}$, and the denominator W expanded in a Taylor series owing to the large size of $[2(\Delta_{\rm hf}+\Delta)/\gamma]^2$ compared to the other terms. This leads to the four-level-model approximate form of the parameter G, which includes the first-order contributions of the $F = 3 \rightarrow F' = 3$ pump light scattering and the repump light scattering as

$$G = \frac{1}{\zeta_{\rm std}}\left[[1+(2\Delta/\gamma)^2]\left(1-2\epsilon\frac{A}{B}\right) + \frac{P}{P_{\rm sat}}\left(1+\epsilon(k-3)\frac{A}{B}\right)\right]. \tag{A9}$$

[1] M. H. Anderson, J. R. Ensher, C. E. Wieman, and E. A. Cornell, Science **269**, 198 (1995).
[2] C. C. Bradley, C. A. Sackett, J. J. Tollett, and R. G. Hulet, Phys. Rev. Lett. **75**, 1687 (1995).
[3] K. B. Davis, M. O. Mewes, M. R. Andrews, N. J. van Druten, D. S. Durfee, D. M. Kurn, and W. Ketterle, Phys. Rev. Lett. **75**, 3969 (1995).
[4] B. DeMarco and D. S. Jin, Science **285**, 1703 (1999).
[5] B. DeMarco, J. L. Bohn, J. P. Burke, M. Holland, and D. S. Jin, Phys. Rev. Lett. **82**, 4208 (1999).
[6] A. G. Truscott, K. E. Strecker, W. I. McAlexander, G. B. Partridge, and R. G. Hulet, Science **291**, 2570 (2001).
[7] F. Schreck, G. Ferrari, K. L. Corwin, J. Cubizolles, L. Khaykovich, M.-O. Mewes, and C. Salomon, Phys. Rev. A **64**, 011402 (2001).
[8] Z. Hadzibabic, C. A. Stan, K. Dieckmann, S. Gupta, M. W. Zwierlein, A. Görlitz, and W. Ketterle, Phys. Rev. Lett. **88**, 160401 (2002).
[9] K. M. O'Hara, S. L. Hemmer, M. E. Gehm, S. R. Granade, and J. E. Thomas, Science **298**, 2179 (2002).
[10] G. K. Campbell, M. M. Boyd, J. W. Thomsen, M. J. Martin, S. Blatt, M. D. Swallows, T. L. Nicholson, T. Fortier, C. W. Oates, S. A. Diddams *et al.*, Science **324**, 360 (2009).
[11] P. D. Lett, K. Helmerson, W. D. Phillips, L. P. Ratliff, S. L. Rolston, and M. E. Wagshul, Phys. Rev. Lett. **71**, 2200 (1993).
[12] J. D. Miller, R. A. Cline, and D. J. Heinzen, Phys. Rev. Lett. **71**, 2204 (1993).
[13] R. A. Cline, J. D. Miller, and D. J. Heinzen, Phys. Rev. Lett. **73**, 632 (1994).
[14] C. Gabbanini, A. Fioretti, A. Lucchesini, S. Gozzini, and M. Mazzoni, Phys. Rev. Lett. **84**, 2814 (2000).
[15] L. Marcassa, V. Nascimento, L. Caliri, A. Caires, D. Magalhes, and V. Bagnato, Laser Phys. **16**, 1722 (2006).
[16] Y. Huang, J. Qi, H. K. Pechkis, D. Wang, E. E. Eyler, P. L. Gould, and W. C. Stwalley, J. Phys. B **39**, S857 (2006).
[17] K. M. Jones, E. Tiesinga, P. D. Lett, and P. S. Julienne, Rev. Mod. Phys. **78**, 483 (2006).
[18] K.-K. Ni, S. Ospelkaus, M. H. G. de Miranda, A. Pe'er, B. Neyenhuis, J. J. Zirbel, S. Kotochigova, P. S. Julienne, D. S. Jin, and J. Ye, Science **322**, 231 (2008).
[19] S. Ospelkaus, K.-K. Ni, M. H. G. de Miranda, B. Neyenhuis, D. Wang, S. Kotochigova, P. S. Julienne, D. S. Jin, and J. Ye, Faraday Discuss. **142**, 351 (2009).
[20] A. Chotia, B. Neyenhuis, S. A. Moses, B. Yan, J. P. Covey, M. Foss-Feig, A. M. Rey, D. S. Jin, and J. Ye, Phys. Rev. Lett. **108**, 080405 (2012).
[21] S. Jochim, M. Bartenstein, A. Altmeyer, G. Hendl, S. Riedl, C. Chin, J. Hecker Denshlag, and R. Grimm, Science **302**, 2101 (2003).
[22] M. W. Zwierlein, C. A. Stan, C. H. Schunck, S. M. F. Raupach, S. Gupta, Z. Hadzibabic, and W. Ketterle, Phys. Rev. Lett. **91**, 250401 (2003).
[23] C. A. Regal, C. Ticknor, J. L. Bohn, and D. S. Jin, Nature (London) **424**, 47 (2003).
[24] R. S. Schappe, T. Walker, L. W. Anderson, and C. C. Lin, Phys. Rev. Lett. **76**, 4328 (1996).
[25] B. J. Claessens, J. P. Ashmore, R. T. Sang, W. R. MacGillivray, H. C. W. Beijerinck, and E. J. D. Vredenbregt, Phys. Rev. A **73**, 012706 (2006).
[26] K. J. Matherson, R. D. Glover, D. E. Laban, and R. T. Sang, Phys. Rev. A **78**, 042712 (2008).
[27] D. E. Fagnan, J. Wang, C. Zhu, P. Djuricanin, B. G. Klappauf, J. L. Booth, and K. W. Madison, Phys. Rev. A **80**, 022712 (2009).
[28] J. Weiner, V. S. Bagnato, S. Zilio, and P. S. Julienne, Rev. Mod. Phys. **71**, 1 (1999).
[29] C. Monroe, H. Robinson, and C. Wieman, Opt. Lett. **16**, 50 (1991).
[30] G. Santarelli, P. Laurent, P. Lemonde, A. Clairon, A. G. Mann, S. Chang, A. N. Luiten, and C. Salomon, Phys. Rev. Lett. **82**, 4619 (1999).
[31] M. Kasevich and S. Chu, Phys. Rev. Lett. **67**, 181 (1991).
[32] J. Schmiedmayer, Appl. Phys. B: Lasers Opt. **60**, 169 (1995).
[33] N. H. Dekker, C. S. Lee, V. Lorent, J. H. Thywissen, S. P. Smith, M. Drndić, R. M. Westervelt, and M. Prentiss, Phys. Rev. Lett. **84**, 1124 (2000).
[34] W. Hansel, P. Hommelhoff, T. W. Hansch, and J. Reichel, Nature (London) **413**, 498 (2001).
[35] T. Schumm, S. Hofferberth, L. M. Andersson, S. Wildermuth, S. Groth, I. Bar-Joseph, J. Schmiedmayer, and P. Kruger, Nat. Phys. **1**, 57 (2005).
[36] P. Bohi, M. F. Riedel, T. W. Hansch, and P. Treutlein, Appl. Phys. Lett. **97**, 051101 (2010).
[37] D. A. Smith, S. Aigner, S. Hofferberth, M. Gring, M. Andersson, S. Wildermuth, P. Krüger, S. Schneider, T. Schumm, and J. Schmiedmayer, Opt. Express **19**, 8471 (2011).
[38] C. Mok, B. Barrett, A. Carew, R. Berthiaume, S. Beattie, and A. Kumarakrishnan, Phys. Rev. A **88**, 023614 (2013).

[39] H. J. Metcalf and P. van der Straten, *Laser Cooling and Trapping* (Springer, New York, NY, USA, 1999).
[40] S. Chang and V. Minogin, Phys. Rep. **365**, 65 (2002).
[41] D. Budker, D. F. Kimball, and D. P. DeMille, *Atomic Phyics* (Oxford University Press, Padstow, Cornwall, UK, 2004).
[42] Y.-C. Chen, Y.-A. Liao, L. Hsu, and I. A. Yu, Phys. Rev. A **64**, 031401 (2001).
[43] D. B. Hume, I. Stroescu, M. Joos, W. Muessel, H. Strobel, and M. K. Oberthaler, arXiv:1307.7598 (2013).
[44] T. Walker, D. Sesko, and C. Wieman, Phys. Rev. Lett. **64**, 408 (1990).
[45] D. W. Sesko, T. G. Walker, and C. E. Wieman, J. Opt. Soc. Am. B **8**, 946 (1991).
[46] T. Pohl, G. Labeyrie, and R. Kaiser, Phys. Rev. A **74**, 023409 (2006).
[47] G. L. Gattobigio, T. Pohl, G. Labeyrie, and R. Kaiser, Phys. Scr. **81**, 025301 (2010).
[48] P. D. Lett, W. D. Phillips, S. L. Rolston, C. E. Tanner, R. N. Watts, and C. I. Westbrook, J. Opt. Soc. Am. B **6**, 2084 (1989).
[49] C. G. Townsend, N. H. Edwards, C. J. Cooper, K. P. Zetie, C. J. Foot, A. M. Steane, P. Szriftgiser, H. Perrin, and J. Dalibard, Phys. Rev. A **52**, 1423 (1995).
[50] C. Gabbanini, A. Evangelista, S. Gozzini, A. Lucchesini, A. Fioretti, J. H. Muller, M. Colla, and E. Arimondo, Europhys. Lett. **37**, 251 (1997).
[51] J. L. Booth, J. Van Dongen, P. Lebel, B. G. Klappauf, and K. W. Madison, J. Opt. Soc. Am. B **24**, 2914 (2007).
[52] K. Ladouceur, B. G. Klappauf, J. Van Dongen, N. Rauhut, B. Schuster, A. K. Mills, D. J. Jones, and K. W. Madison, J. Opt. Soc. Am. B **26**, 210 (2009).
[53] D. A. Steck, http://steck.us//alkalidata (rev. 0.2.1).